Journal of Sea Research
In Press
http://dx.doi.org/10.1016/j.seares.2011.04.009

Modelling growth variability in longline mussel farms as a function of stocking density and farm design

Rune Rosland[a, *], Cédric Bacher[b], Øivind Strand[c], Jan Aure[c] and Tore Strohmeier[c]

[a] Dept. of Biology, University of Bergen, Postbox 7800, 5020 Bergen, Norway
[b] Ifremer, Centre de Brest, BP 70, Z.I. Pointe du Diable, 29280 Plouzané, France
[c] Institute of Marine Research, PO Box 1870 Nordnes, 5817 Bergen, Norway

[*] Corresponding author : R. Rosland, Tel.: + 47 55584214, email address : rune.rosland@bio.uib.no

Abstract:

The simulations demonstrate spatial growth patterns at longlines under environmental settings and farm configurations where flow reduction and seston depletion have significant impacts on individual mussel growth. Longline spacing has a strong impact on the spatial distribution of individual growth, and the spacing is characterised by a threshold value. Below the threshold growth reduction and spatial growth variability increase rapidly as a consequence of reduced water flow and seston supply rate, but increased filtration due to higher mussel densities also contributes to the growth reduction. The spacing threshold is moderated by other farm configuration factors and environmental conditions. Comparisons with seston depletion reported from other farm sites show that the model simulations are within observed ranges. A demonstration is provided on how the model can guide farm configuration with the aim of optimising total farm biomass and individual mussel quality (shell length, flesh mass, spatial flesh mass variability) under different environmental settings. The model has a potential as a decision support tool in mussel farm management and will be incorporated into a GIS-based toolbox for spatial aquaculture planning and management.

Research highlights

► New model for flow reduction, seston depletion and mussel growth in longline farms. ► Integration of processes at the level of individual mussels and at the farm level. ► Mussel size and condition depend on farm configuration and environment. ► Spacing between longlines is the most influential farm parameter on mussel growth. ► The effects of farm configuration are moderated by environmental conditions.

Keywords: Longline farm configuration; Environmental conditions; Flow reduction; Seston depletion; Spatial growth variability

1. Introduction

Mussels (*Mytilus edulis*) are commonly cultivated on artificial structures like rafts, poles or longlines to facilitate farming operations. The production potential of a mussel farm is defined by the environmental background conditions, while the realised production depends on how the farm is scaled and configured with respect to the environmental factors.

Longline farms are relatively simple constructions comprised by two or more parallel lines at the sea surface to which a series of vertically oriented ropes (or loops from a single rope) are attached (Fig. 1). The vertical ropes provide settling and grow out substrate to the mussels. The stocking density per longline is given by the number of mussels per meter rope, the frequency of ropes per longline and the depth of the ropes. The longlines are usually oriented parallel to the dominating current directions so that water can flow through the channels delimited by the longlines and the vertical ropes (Fig. 1). Due to friction with farm structures and filtration by the mussels both water flow and seston concentration decrease downstream of the flow direction (Aure et al., 2007). Flow reduction (Blanco et al., 1996; Boyd and Heasman, 1998; Heasman et al., 1998; Petersen et al., 2008; Pilditch et al., 2001; Stevens et al., 2008) and seston depletion (Karayucel and Karayucel, 2000; Maar et al., 2008; Petersen et al., 2008; Strohmeier et al., 2005; Strohmeier et al., 2008) have been observed in both rafts and longline systems. Persistent spatial differences in food supply will likely be reflected as spatial differences in mussel growth (Aure et al., 2007; Strohmeier et al., 2005; Strohmeier et al., 2008).

Current speed, current direction and seston concentration are key environmental factors to which a mussel farm should be configured. Variables like the length of longlines, the spacing between longlines and stocking density are amongst the most important factors that the farmer can manipulate to optimise farm configuration relative to the environmental background conditions. Sub-optimal configurations may lead to seston depletion, reduced mussel growth and increased growth variability in a farm, or in the opposite case, to an under-utilisation of the production potential at the farm site.

A common measure for farm performances is the carrying capacity, but as stated by McKindsey et al. (2006) this concept lacks a clear and concise definition and may have different meanings depending on the context. Inglis et al. (2000) suggested four different definitions of carrying capacity with references to the physical, production, ecological and social levels and scales of aquaculture. The implementation of models and monitoring systems for the improvement of aquaculture can then be reviewed according to such a classification. Model objectives usually focus on some specific issues - *e.g.* assessment of aquaculture impact on the ecosystem functioning, computation of biological production and economic profit, assessment of site suitability, understanding of key biological and physical processes. Some recent models have attempted to account for interactions between different levels and scales, like individuals and populations (Bacher and Gangnery, 2006; Bacher et al., 2003; Brigolin et al., 2009; Brigolin et al., 2008; Duarte et al., 2008), populations and ecosystems (Cugier et al., 2010; Filgueira and Grant, 2009), and individual, populations and ecosystems (Ferreira et al., 2008). Ferreira et al. (2008) even included measures of production and ecological carrying capacity in an advanced model for mussel farm management, which encompassed physical, biological and economic factors.

However, as stated by McKindsey et al. (2006) the assessment of carrying capacity by models at higher levels of complexity relies on a thorough understanding of the direct interactions between farms and environment. As such, one of the challenges in mussel cultivation is how to scale and configure farms in order maintain an overall high production rate and quality of individual mussels, and at the same time reduce the spatial variability of these variables within the farm. To account for these measures a functional definition of production carrying capacity (Inglis et al., 2000) should include *e.g.* thresholds for the size and condition of mussels and the spatial variability of these. Modeling optimal farm configuration based on these criteria requires models which integrate growth and energetics at the scale of individual mussels with processes at the farm scale, like the spatial distribution of water flow and food concentrations.

This paper focuses on the production capacity of longline mussel farms and presents a dynamic model able to assess new criteria related to spatial distribution of mussel size and condition inside a longline farm as a function of farm configuration and environmental background conditions. The model combines an existing model for simulation of water flow reduction (Aure et al., 2007) and seston depletion inside longline farms (Aure, unpublished) with a Dynamic Energy Budget (DEB) model for blue mussels (Rosland et al., 2009). The model for water flow and seston depletion has been validated on data from farms in Western Norway (Aure, unpublished), while the DEB model has been validated on mussel growth data from sites in Western and Southern Norway (Rosland et al., 2009).

The main objectives are to: 1) Demonstrate the model and its application to longline farms, 2) Simulate seston depletion inside a longline farm and assess the sensitivity of individual mussel growth and spatial growth variability to farm configuration and background environmental conditions, 3) Provide guidelines for farm configuration based on production criteria like shell length, flesh weight, and spatial variability in shell length and weight.

2. Materials and Methods

The farm model presented here combines two existing models: 1) A steady-state model for water flow reduction (Aure et al., 2007) and seston depletion (Aure, unpublished) in longline farms, and 2) A DEB model for individual blue mussels (Rosland et al., 2009) based on DEB theory (Kooijman, 1986, 2000) and previously developed models for oysters (Pouvreau et al., 2006) and mussels (van der Veer et al., 2006). A further description of the model for flow reduction and seston depletion is provided in Aure et al. (2007) and in the Annex, while a further description and background of the DEB model can be found in Rosland et al. (2009). The following text will focus on the equations describing the coupling of the two models.

2.1 The model

The concept of the model is illustrated in Fig. 1. It is assumed that the physical properties are identical along the longline corridors, that water flows parallel to the longlines, and that the friction with farm structures gradually reduces the current speeds downstream of the flow direction (Annex). It is assumed that the combination of reduced water flow and seston filtration along the longlines produces a decreasing seston concentration gradient in the flow direction.

The longline is divided into a number (N) of equal segments of length B_L, which together with the spacing of longlines (B_W) and depth of the ropes (B_H) confine a set of N boxes with fixed volumes (B_V) along the longlines (Fig. 1). The current velocity at the exit of box n can be calculated as:

$$v_{n+1} = v_1 \cdot \left(\frac{1 - \dfrac{f_K \cdot B_L}{B_W}}{1 + \dfrac{f_K \cdot B_L}{B_W}} \right)^n \qquad (1)$$

where f_K is the friction coefficient and v_1 is the background current velocity (*i.e.* at the entry of the box). Seston concentration S_{n+1} (mg m^{-3}) at the exit of box *n* results from the mass balance between inflow, outflow and filtration by mussel (Fig. 1). We write:

$$S_{n+1} = S_n \left(B_A \cdot (v_n + v_{n+1}) - F_n\right) / \left(B_A (v_n + v_{n+1}) + F_n\right) \qquad (2)$$

where B_A is the area of the box opening (B_A=$B_W\,B_H$), v_n and v_{n+1} are the current speeds at the entrance and exit of box *n*, respectively, and F_n is the total clearance rate in box *n*. F_n is related to the box volume B_V (m^3), individual clearance rate C_r (m^3 d^{-1} ind^{-1}) and the density of mussels M_n (ind m^{-3}) in box *n* by:

$$F_n = B_V C_r M_n \qquad (3)$$

Eqs 1-2 describes the discrete steady-state model for seston depletion caused by water flow reduction and seston filtration.

The model for flow reduction and seston depletion is coupled with the DEB model for mussel growth at the term for total clearance rate (F_n). In the coupled model this term is calculated from the food ingestion rate $\dot{p}_X$ (J d^{-1}) in the DEB model:

$$\dot{p}_X = \{\dot{p}_{Xm}\} f V^{2/3} \qquad (4)$$

where $\{\dot{p}_{Xm}\}$ is the maximum ingestion rate per surface area (J cm^{-2} d^{-1}) of individual mussels, *f* is the scaled functional response moderating feeding rate to ambient seston concentration *S*, and *V* is the structural body volume of a mussel. The functional response is calculated by a Michaelis-Menten function with S_K (Tab. 1) as the half-saturation coefficient (mg chl *a* m^{-3}):

$$f = \frac{S}{S + S_K} \qquad (5)$$

The individual clearance rate (m^3 d^{-1} ind^{-1}) is calculated from the ingestion rate by:

$$C_r = \frac{\dot{p}_X k_J}{S + S_K} \qquad (6)$$

where k_J is a conversion factor from Joule to chlorophyll *a* (chl *a*) ($k_J = 4.2 \cdot 10^{-4}$ mg chl *a* J^{-1}). k_J is the inverse product of the energy per unit Carbon in phytoplankton (11.4 Cal mg^{-1} Carbon) from Platt and Irwin (1973), the Carbon:chl *a* ratio (50:1) in phytoplankton and the ratio between Calories and Joule (4.19 J Cal^{-1}).

The DEB model calculates growth over a series of discrete time intervals where the sequence produces a dynamic growth trajectory for the mussels. However, within each time interval it is assumed that water flow and seston filtration reach steady-state. To ensure the validity of this assumption the duration of the time interval was set to one day, which is larger than the flow through time in the farm. The calculation of ingestion rate (Eq. 4) during a time interval is based on the seston concentration (S) in a box at the beginning of the time interval, while seston concentrations are updated each time interval (Eq. 2) based on the total clearance rate calculated in Eq. 3.

The energy ingested by the mussels (Eq. 4) first enters a reserve compartment from which it is allocated to structural and reproductive growth according to the kappa rule (Kooijman, 2000). All processes are regulated by ambient water temperature according to the Arrhenius function.

2.2 Environmental data

The datasets used to force the model is based on data from Hardangerfjord and Lysefjord, which are both located in the western part of southern Norway. Hardangerfjord (60°6′N, 6°0′E) is 179 km long and has a maximum depth of 800 m, while Lysefjord (59°0′N,6°16′E) is about 40 km long and 400 m deep. The dataset from Lysefjord was applied to demonstrate the coupled farm model with reference to previous studies of flow reduction (Aure et al., 2007) and seston depletion (Aure, unpublished) and observations of spatial growth patterns in farms from this fjord (Strohmeier et al., 2005; Strohmeier et al., 2008). The dataset from Hardangerfjord was applied to demonstrate the effects of seasonal and spatial differences in environmental factors inside a representative fjord of Norway.

2.2.1 The Lysefjord dataset:

This dataset provides similar values to those applied in Aure (unpublished) and Aure et al. (2007) with constant values for chl *a* (1.4 mg m^{-2}), current velocity (6 cm s^{-1}) and water temperatures (10.7 °Celcius). The values are based on data presented in (Strohmeier et al.,

2005) and a further description of the data collection program and methods can be found there.

2.2.2 The Hardangerfjord dataset

This dataset provides seasonal values for chl *a*, current velocity and temperatures. The environmental data were collected during the years 2007-2008 (Husa et al., 2010) at cross sections from the head to the mouth of the fjord. The data include water temperatures and chl *a* which were simultaneously measured using a CTD-probe (SAIV SD204, http://www.saivas.no). Fluorescence units were converted to chl *a* concentration using a calibration obtained from analysis of water samples and according to the equation: mg chl *a* m^{-3} = (0.84·fluorescence) – 0.12; (r^2 = 0.93, n = 33). Samples were taken every month, but not at all the stations every time. Linear interpolation between observation dates was applied to create a dataset with daily resolution. Current velocities were measured by Aanderaa Instruments doppler current sensors 4100 (http://www.aadi.no). Currents were recorded every hour at 11 meter depth on the two stations (http://talos.nodc.no:8080/observasjonsboye/) for approximately half a year each, and the data series were repeated in the model data setup to cover a full year.

In order to test the farm model within the observed ranges of chl *a* and currents in the Hardangerfjord we established two data sets based on the outer ranges of chl *a* and current speeds, while the temperature is based on the monthly averages between all stations:

*2.2.2.1 Hardanger HIGH***:**

This dataset is composed of the maximum chl *a* concentrations observed amongst the fjord stations each month, and the current dataset with the largest velocity amplitudes (Fig. 2). The temperature is composed of the average value of all stations for each month.

2.2.2.2 Hardanger LOW:

This dataset is composed of the minimum chl *a* concentrations observed amongst the fjord stations each month, and the current dataset with the least velocity amplitudes (Fig. 2). The temperature is composed of the average value of all stations for each month.

2.3 The simulations

Unless specified, all the simulations are based on the standard farm parameters listed in Tab. 1. The friction coefficient f_K of 0.02 was based on data from the farm in Lysefjord (Aure et al., 2007; Strohmeier et al. 2005), and has been further validated by measurements inside several farms giving a strong relationship between observed and estimated current speed (f_K = 0.02) (n=13, r^2=0.9) (Aure, unpublished). The stocking density at the longline is defined by the parameter *nmussel* (Tab. 1). It has the unit ind m^{-2} and refers to the number of mussels per square meter area which is confined by the longlines and the vertical ropes (Fig. 1). A mussel density of 500 ind m^{-1} vertical rope and a distance of 0.5 m per rope attached to the longlines would thus be equivalent to a longline stocking density of 1000 ind m^{-2}. Stocking density at the longlines is fixed by the stocking parameter, which means that the mussel density (ind m^{-3}) varies inversely proportional to the spacing between longlines.

This paper presents the results from four simulation setups:

1. **Background current directions and longline spacing:** These simulations are forced by the Lysefjord dataset and demonstrate the spatial patterns of water flow, chl *a* concentrations and mussel flesh mass inside a farm resulting from different combinations of longline spacing (1-10 m) and background currents (one-directional currents; two-directional currents with a 1:1 distribution of directions; and two-way currents with a 3:1 distribution of directions).
2. **Environmental factors and farm configuration:** These simulations are forced by the Lysefjord dataset and demonstrate how the growth of mussels responds to changes in farm configuration (longline spacing, reduced farm length, reduced stocking density at longlines) and environmental factors (chl *a* concentration and current velocity).
3. **Growth simulations on realistic ranges of environmental forcing data:** These simulations demonstrate the growth response in mussels within the ranges of chl *a* and currents in the Hardangerfjord (HIGH and LOW) at different longline spacing alternatives.
4. **Optimising farm configuration based on multiple criteria:** These simulations demonstrate how the model can be used to optimize the configuration of farm length, longline spacing and stocking density in order to maximise farm biomass and at the same time satisfying the criteria for mussel lengths (>28 mm), flesh weight (>0.45 g WW) and spatial flesh weight variability (<10% standard deviation divided by mean flesh weight) inside the farm. The simulations are based on the datasets Hardanger HIGH and Hardanger LOW.

2.4 Depletion index

The model was used to derive a Depletion Index and compare performance of different mussel farms and configurations in different environmental conditions. Guyondet et al. (2005) refer to the definition of depletion by Dame and Prins (1998), which is based on the comparison between three different time scales: phytoplankton turnover time (*TT*), bivalve clearance time (*CT*) and water renewal time (*RT*). *TT* corresponds to the time taken for the phytoplankton to be renewed through primary production, which we neglected in our study. For instance a high ratio *CT*/*RT*, while *TT* remains large, would result in a low depletion due to the fast renewal of water (small *RT*) compared to the capacity of bivalves to filter and remove particles (high *CT*). On the opposite, a large effect of bivalves on food concentration would result from a low CT/RT. Petersen et al. (2008) measured food concentrations (or a proxy using fluorescence or chl *a*) at three different spatial scales and defined depletion ratio as the relative difference between values taken 20 to 30 m upstream of the raft and inside the raft (macro-scale), just in front of the leading edge of the raft (meso-scale), or between ropes (micro-scale). They also derived depletion rates from the slope of the linear regression between the concentration of chl *a* and the distance, on a log-scale, inside a raft. At a larger scale Simpson et al. (2007) also measured and simulated longitudinal profiles of chl *a* along a mussel bed, using a transport equation similar to the one we used in this study (completed with a primary production term) and, there again, the depletion was related to the differences between concentration inside and outside the area of interest.

In the following we will keep to the definition of the depletion index as:

$$DI = \frac{RT}{CT}$$

Thus a high value of the index indicates a high level of depletion. In the Annex we show that there is some relation between this index, the rate of decrease in the farm area and the ratio between the concentrations at both edges of the farm.

We have reviewed several published studies where this index could be computed at the meso-scale defined by Petersen et al. (2008). Our objective was to compare different types of cultivation systems (rafts, longlines) with their own spatial dimensions, current speeds and bivalve densities, and assess in which cases depletion would occur (Tab. 2). Regarding our model, we integrated current velocity and mussel clearance rate over time and space in order to compute an average depletion index. We carried out these calculations for two contrasted scenarios based on distance between adjacent longlines equal to 1 and 10 m, and length of longlines equal to 300 m.

3. Results

3.1 Simulations 1: Background current directions and longline spacing

The results from the simulations with standard farm parameters (Tab. 1) and the Lysefjord dataset are presented in Fig. 3, which shows the mean (over the simulation period) current speeds and chl *a* concentration and final mussel flesh mass at different longline positions. The vertical bars for the case with 3 m spacing between longlines shows the temporal variability in currents and chl *a* concentrations over the simulation period

For the case with one flow direction (Fig. 3, left column) current speeds, chl *a* concentrations and mussel growth follow decreasing gradients downstream of the current direction. Spacing between longlines has a strong impact on the steepness of these gradients and the longline positions where the flow reaches 50 % of the inflow speed corresponds to approximately 250, 100 and 50 m for longline spacing distances of 10, 5 and 1 m, respectively. The chl *a* trajectories follow a similar pattern, but there seem to be an inflection point at about 3 m longline spacing. For spacing above 3 m the depletion is moderate while below the depletion escalates rapidly with decreasing spacing. At 10 m spacing the concentrations reaches about 80% of the inflow values at the downstream end of the farm (300 m), while at 5 m and 1 m spacing the concentrations reaches 50% of the inflow value at about 250 and 80 m, respectively. The spatial distribution of mussel flesh mass by the end of the simulation period reflects the chl *a* profiles.

For the case with symmetrically alternating current directions (Fig. 3, middle column) water flow distributions reaches a minimum at the centre of the longline, but the difference between central and edge positions of the longlines are now less than in the one-directional case. The spatial chl *a* profile is different from currents. At longline spacing below 3 m the chl *a* minimum occurs at the centre of the longline, while for spacing above 3 m the situation is opposite with the chl *a* maximum at the centre of the longline. The spatial patterns of mussel flesh mass reflects the chl *a* concentrations except for the case with 3 m spacing, where mussel mass has a distinct maximum at the centre of the longline. The temporal variability (shown for the 3 m case) is at maximum at the edge positions, as expected due to the alternating current directions.

The simulation with non-symmetrically (3:1) alternating current directions is shown in the right column of Fig. 3. The spatial patterns and temporal variability are in-between the cases with one-directional and symmetrical currents.

Final mussel flesh mass and temporal variability in chl *a* is plotted against the temporal mean chl *a* concentrations in Fig. 4 for the simulation with symmetrically alternating current directions. In general the final mussel flesh mass increases in proportionally to mean chl *a* concentration except for the spatial positions where the mean chl *a* concentrations range between 0.5-0.8 mg m^{-3}. Here the final mussel mass becomes less at positions with high temporal chl *a* variation (edge positions) compared with positions with low temporal chl *a* variation (middle positions). The reason for this is that the lower part of the chl *a* variability range enters the lower linear parts of the functional response curve (Eq. 4) where the feeding rate drops quickly towards zero, which thus pulls the mean feeding rate down at these longline positions.

3.2 Simulations 2: Environmental factors and farm configuration:

The simulation of mussel growth at different spacing between longlines at different combinations of farm length and stocking density are displayed in the upper left panel of Fig. 5. The standard refers to the simulation with standard farm parameters and the Lysefjord forcing data. The graph shows mean flesh mass in the farm (lines) and spatial variability between line-positions (bars). For longline spacing below 6 m a reduction in farm length or stocking density result in increased mean flesh mass, while the effect is modest and decreasing at larger spacing alternatives. The model is most sensitive to changes in farm length and results in a doubling of mussel mass at the shortest spacing alternatives. The spatial variability is largest at 1-6 m line spacing.

Farm biomass (lower left panel in Fig. 5) decreases with increasing longline spacing due to dilution of the stocking density. However, at short longline spacing (below 3-4 m) the increase in individual growth with increasing spacing compensates for the reduction in stocking density. Shorter farms also result in larger final biomass (kg m^{-3}) due to higher individual growth.

Simulation of mussel growth at different longline spacing and combinations of background chl *a* concentration and current speeds are displayed in the upper right panel of Fig. 5. The mussel growth is most sensitive to a doubling of chl *a* concentrations, while a doubling of background currents has moderate effects compared with the standard run. The farm biomass is shown in the lower right panel of Fig. 5 and the strong response to doubled chl *a* concentrations is due to increased individual growth.

3.3 Simulations 3: Growth simulations on realistic ranges of environmental forcing data:

Simulations of spatial mussel growth and farm biomass at different combinations of chl *a* concentrations, current speeds and line spacing are displayed in the left column of Fig. 6. The forcing data used are the Hardanger HIGH and Hardanger LOW.

Chl *a* concentration has the strongest impact on mussel growth and the HIGH concentration more than doubles the mussel growth compared to the LOW concentration. Background currents has less effect and the difference in mussel flesh mass between the HIGH and the LOW current dataset is about 30% at the maximum. Besides, the difference between the two current regimes diminishes as line spacing increases, while the differences caused by different background chl *a* concentrations remain, irrespectively of line spacing alternatives. The farm biomass reflects the changes in individual mussel mass under the different environmental regimes.

The right side panels in Fig. 6 displays simulated mussel growth and farm biomass based on the same environmental forcing data, but without the flow reduction function (*i.e.* friction is set to zero and only filtration by mussels can cause seston depletion). It clearly illustrates the impact from flow reduction on mussel growth at the shortest longline spacing alternatives (< 6 m).

3.4 Simulations 4: Optimising farm configuration based on multiple criteria

The results from the simulations of farm biomass at different farm configurations (length of longline, spacing between longlines and stocking density at the longline) and background concentrations of chl *a* are displayed in Fig. 7. The isoclines indicate how the density of farm biomass (kg m^{-3}) changes with different combinations of farm length (*x*-axis) and longline spacing (*y*-axis), while the shaded area indicates which combinations will result in an individual size and/or size variability that are not in compliance with the criteria. The general pattern is that biomass density (isoclines) changes inversely with farm length and spacing between longlines. The exception is when spacing distances are within the ranges where individual mussel mass increases with line spacing, and hence compensates for the biomass reduction from reduced stocking density in the farm (as explained in connection with Fig. 5). The upper left diagram (Fig. 7) shows the case with high background chl *a* and low stocking density at the longline. For longlines below 120 m length the criteria are withheld for all line spacing alternatives, while above 120 m the corresponding longline spacing must be kept above the grey area to keep mussel size and size variability within the criteria (*e.g.* a farm of 600 m length must therefore keep line spacing above 5 m).

The upper right diagram shows the case with both low background chl *a* and low stocking density at the longline. Due to decreased individual growth the farm biomass density (isoclines) decreases to about half the level compared to the case with high background chl *a*. This is also reflected by the enlarged grey area which indicates more restriction on the combinations of longline spacing and line lengths which satisfies the criteria (*e.g.* 100 m line length requires line spacing > 2 m, 350 m line length requires line spacing > 10 m).

The lower left diagram shows the case with both high background chl *a* and high stocking density at the longline. Compared with the low stocking case (upper left diagram) the density of biomass (isoclines) is almost doubled due to the density of mussels. Higher density also reduces the individual growth which increases the restrictions of line length and spacing combinations (grey area) which satisfy the criteria (*e.g.* 100 m line length requires line spacing > 2 m, 600 m line length requires line spacing > 7 m).

The lower right diagram shows a case with low background chl *a* and high stocking density at the longline. The low individual growth resulting from the combination of low food and high stocking density puts strong restrictions (grey area) on the acceptable combinations of line length and spacing (e.g. 100 m line length requires line spacing > 5 m, 250 m line length requires line spacing > 10 m).

3.5 Depletion index

Calculations show a wide range of Depletion Indices (Tab. 2). Values above or close to 1 are found for one case in Bacher et al. (2003) and Heasman et al. (1998), for one of the two cases in Heasman et al. (1998) and Strohmeier et al. (2008) and in this study (for a distance between longlines equal to 1 m). All these cases correspond to sites where current velocities are very low (a few cm s^{-1}) and concern rafts as well as longlines. On the opposite, the lowest Depletion Index are met in Guyondet et al. (2010), Pilditch et al. (2001), Plew et al. (2005) and Sara and Mazzola (2004) where the density of mussels is low, or sites where current velocity is high (one case in Bacher and Black (2008) and Bacher et al. (2003). In our study, the calculation has been applied to cases corresponding to Hardanger HIGH scenarios with low/high spacing between longlines and the contrast illustrates the inverse relationship between Depletion Index and growth. In the first case (spacing=1 m), Depletion Index was equal to 4.3 and mussel growth was equal to 1 g (Fig. 7). In the second case (spacing=10 m), Depletion index was equal to 0.2 and mussel growth was equal to 1.6 g (Fig. 7)

4. Discussion

The results presented here demonstrate the importance of farm configuration in relation to environmental background conditions. The spacing between longlines is a key parameter for the performance of a longline farm with respect to total biomass production and individual mussel growth. Our results indicate that there exist a threshold value for line spacing below which the effects of flow reduction and filtration escalate rapidly and result in strong reductions of individual mussel growth and increased growth variability at the longlines. Above the threshold the effect of line spacing has moderate influence on individual growth and it diminishes as spacing distance increases. The value of the spacing threshold depends on other factors like farm length and environmental conditions as seen in Fig. 5. The simulations based on the Lysefjord and Hardangerfjord data indicate a spacing threshold about 2-4 m (Figs 5-6). The simulations with and without flow reduction showed clearly that flow reduction is the most important factor for growth reduction and growth variability when longline spacing is below the threshold, while beyond the threshold the background conditions becomes more dominating as the farm effects fade off.

The density of biomass in a farm is the product of individual mass and stocking density, but as illustrated in Figs 5-6 the contribution from each of these components relies on the spacing between the longlines. The maximum density of biomass occurs at about 2-4 m spacing (optimum) depending on the simulation settings. Below optimum spacing the potential increase in biomass from higher mussel density is countered by the decrease in individual growth, while above optimum spacing the potential increase in farm biomass from increased individual growth is countered by the reduced mussel density.

The mussel farmer cannot rely on measures on farm biomass density only, since this may camouflage important qualitative aspects of the mussel stock, such as the size and condition of mussels and the spatial variability of these variables. The results presented in Fig. 7

demonstrate that many possible combinations of farm length and line spacing, which from a biomass density perspective looks fine, turns out to be unacceptable from the perspective of individual mussel quality. These results also demonstrate the benefits of including processes at the farm scale (population biomass, size variability) and at the individual scale (size, condition) in models aimed at planning and management of mussel farms. The model could potentially be integrate with bio-economic model like e.g. Ferreira et al. (2007) to bring in spatial aspects of mussel growth and quality into economic models for the maximisation of profits in farms.

The model for flow reduction (Aure et al., 2007) and seston depletion (Aure, unpublished) and the DEB model for mussels (Rosland et al., 2009) has been validated separately against field data, but currently we do not have access to suitable data to validate the coupled farm model presented here. Thus, in the following discussion we will attempt to compare general patterns predicted by the model with patterns observed in longline and raft systems as a preliminary “ground-truthing” of the model. However, a recently started project in St. Peters Bay in Canada aims to establish data that can be used for a more thorough validation of the coupled farm model.

4.1 Water flow and flow reduction

The interference between water and the physical structures of the farm (including the mussels) is one of the core processes in this model. The physical obstruction by farm structures can force the flow into new directions and reduce flow speed through friction. This model accounts for the frictional processes which leads to a reduction in flow speed and a loss of surplus water masses below the farm (Aure et al., 2007). Aure et al. (2007) suggested that mussel size and distance between the suspended mussel ropes on the long line are likely determinants for friction properties, and since the friction coefficient can only be empirically determined and substantially contribute to uncertainty, there is need for quantifying the influence of main determinant factors for friction properties if modeling current speed reduction in mussel long-line farms is to be improved.

Flow reduction has been observed in longline farms (Plew et al., 2006; Strohmeier et al., 2005; Strohmeier et al., 2008) and the average flow patterns is characterised by weaker flow in the central part and stronger flow at the edge positions of the farm (Strohmeier et al., 2005; Strohmeier et al., 2008). An assumption of this model is that the background current direction is parallel to the longlines, which may be realistic with respect to mean currents, but a longline farm will also be exposed to non-parallel background currents which presumably could change the spatial flow distribution in the farm. However, observations from longline farms (Strohmeier et al., 2008) and mussel rafts (Boyd and Heasman, 1998) seems to indicate that background currents do align to the structures inside the farm.

Flow reduction has also been observed under mussel rafts (Blanco et al., 1996; Boyd and Heasman, 1998; Heasman et al., 1998; Petersen et al., 2008; Pilditch et al., 2001; Stevens et al., 2008). Heasman et al. (1998) also observed that higher density of ropes increases the flow reduction in the farm, which is in accordance with the formulation of friction in this model. Plew et al. (2006) argued that the flux of food particles in longline mussel farms is a function of spacing between mussel ropes and the spacing of the longlines. The internal geometric shape of the farm is also important and studies by Aure et al. (2007) and Pilditch et al. (2001) showed that alternations in the width to length ratio of farms can optimise the seston supply. The simulations presented here is in compliance with previous studies and the impacts from farm configuration is evident from the changes in mussel growth in Figs 5-7.

Spatial distribution of flow inside and around farm structures is, however, complex and may also involve changes of current directions as well as local speedups of flow in or around farm structures (Stevens et al., 2008). Factors like stratification, which are not considered here, can influence the flow dynamics in and around farms (Plew et al., 2006). Dense populations of mussels are capable of pumping large amounts of water, which could potentially interfere with water flow at a smaller scale. However, studies by Plew et al. (2009) concluded that the drag from mussel feeding could be ignored compared to the drag effects caused by the farm structures.

Since water carries food particles to the mussels the strength and directions of flow inside a farm is expected to have a major influence on the individual growth and spatial growth distribution of mussels. Although this model only considers parallel (to the longlines) flow directions, the results presented in Fig. 3 clearly demonstrate how flow directions in combination with flow reduction influence the spatial size distribution of mussels in a farm.

4.2 Seston depletion and mussel growth

Flow reduction and filtration by the mussels reduce the food supply rate to downstream longline positions. Over time this will emerge as spatial differences in mussel size and condition factors in the farm. Seston depletion over shellfish beds and inside farms has been observed at different geographic scales. Studies of mussel raft systems (Karayucel and Karayucel, 2000; Maar et al., 2008; Petersen et al., 2008) have shown that the food particle concentrations are significantly lower at the outlet or downstream areas of mussel rafts compared to the background levels. Studies of longline farms (Strohmeier et al., 2005; Strohmeier et al., 2007) showed a sharp decrease in downstream seston concentrations. Seston depletion has been demonstrated indirectly via growth studies like in Fuentes et al. (2000) who observed weaker mussel growth downstream farm positions. The large filtering capacity of shellfish has also been shown to affect seston concentrations at the scale of bays in systems with dense aggregations of shellfish (Dolmer, 2000; Grant et al., 2007; Simpson et al., 2007; Tweddle et al., 2005).

Heasman et al. (1998) observed that food depletion through rafts increased with decreasing spacing of the ropes and that a higher fraction of the mussels reached market size as rope spacing increased. This could be a result of improved flow (seston supply) and/or reduced filtration by mussels due to lower stocking densities. However, they also observed that the degree of seston depletion increased with the age (*i.e.* size) of mussels, which is more likely a result of higher filtration capacity amongst the mussels. Drapeau et al. (2006) also observed that growth variability increased with stocking densities in rafts.

These observed links between seston depletion and factors like farm configuration, mussel size and stocking density are in agreement with the mechanisms of our model, which describes filtration capacity as a function of mussel size. Thus the model accounts for temporal and spatial dynamics in the size structure of mussels in the farm, which represents a biological feedback mechanism that can enforce the spatial variability in mussel size and condition factor.

4.3 Other processes

The model presented here only accounts for the transport and consumption of external food particles and ignores recycling of faeces and pseudo-faeces inside the farm. Since the model apply filtration rate and not clearance rate in the calculation of food depletion the exclusion of pseudo-faeces recycling probably has minor effects. Faeces recycling on the other hand could potentially moderate the negative growth in the downstream locations of the farm, particularly in a low seston environment like the Norwegian fjords.

Reduced water flow reduces the ability to keep particles in suspension and sedimentation of larger particles could thus potentially increase the depletion gradient downstream. Increased sedimentation of organic particles due to mussel farms has been documented in several studies (Callier et al., 2006; Carlsson et al., 2009; Giles et al., 2006; Mallet et al., 2006; Mitchell, 2006) but the amount coming from mussels (faeces and pseudo-faeces) or from other particles has not been quantified. Such processes would also be sensitive to different size spectrum of food particles, *e.g.* large and small algae species, which could turn out differently at different sites and at different periods of the growth season.

A model for optimisation of farming practices should also acknowledge economic factors, since economic yield is the ultimate goal in aquaculture. Including the cost of production efforts and maximising net economic gain of production would yield a different solution than a maximisation of biological production only. However, the predictions on spatial variability in mussel biometrics and condition are missing in farm scale models, like *e.g.* Ferreira et al. (2007), and could well be implemented to account for these effects on economic variables.

Our model only consider impacts from the surrounding environment on farm scale carrying capacity aspects, while its interactions with the environment may also include altered seston concentration and composition and nutrient cycling (Dowd, 2005; Jansen et al., in press) which in turn may interact with adjacent farms downstream. This needs to be addressed when carrying capacity at ecosystem scale is considered and a next step could be to integrate the current farm model into ecosystem models to account for potential interactions between farms and environment at different spatial and temporal scales.

4.4 Depletion index

The calculation of a Depletion Index reflects the observed or calculated decrease of food concentration inside the farm area for a wide range of documented studies and is a way to compare shellfish farm performance. For instance, Petersen et al. (2008) found a depletion of chl *a* inside the raft corresponding to ~80% of the outside concentration. They also calculated depletion rates from the measured profiles of concentration of chl *a* as a function of distance and obtained results from 0.03 and 0.39. Their observations were in accordance with levels of phytoplankton reduction of ~30% from mussel rafts in Spanish rías reported in other studies, which is sufficient to result in a Depletion Index ranging from low (~0.30) to medium (~0.75). Plew et al. (2005) explained the low depletion pattern in their study by the low value of the clearance rate compared to the estimated flow rate through the farm. Sara and Mazzola (2004) found that the current velocity is a limiting factor on one site only and would not permit further development of bivalve cultivation, which results in a Depletion Index close to 0.4 when calculated for one farm configuration. On the other studied site, they concluded that the hydrodynamics and the available food would not limit the expansion of bivalve culture due to sufficient water flow and the Depletion Index was smaller than in the first case. A Depletion Index around 0.4 or higher is an indicator of shellfish farms with a potential depletion effect.

Depletion clearly results from a combination of factors – e.g. farm size, bivalve density, and current velocity. Therefore, within the same environmental conditions, the dimension of the farm would yield a more or less pronounced depletion, which is clearly visible in our comparative analysis. For instance Pilditch et al. (2001) predicted a reduction in seston concentration less than 5% within the actual lease size and showed that expanding the lease would reduce the seston concentration in the centre of the lease by 20–50%, hence emphasizing the importance of optimising farm dimensions. They also emphasized the need to better understand whether the reduction of food would affect the growth of cultivated bivalves. It is very clear for our coupled model that this not always the case, since the background concentration may be high enough to sustain growth even if the concentration is reduced inside the farm. An additional criterion would therefore be the ratio S/S_K (where S_K is the half-saturation coefficient used in the DEB model) which reveals the potential limitation of food concentration on growth. This is demonstrated by our simulations with different environment scenarios where mussel growth is limited by a combination of high food depletion and low food concentration corresponding to S/S_K ratios below 0.5 (Tab. 2).

By construction, the Depletion Index is very sensitive to low or high values of *CT* and *RT*. *CT* and *RT* are most often roughly estimated since environmental conditions, current velocity and filtration by mussels vary over time. Depletion Index is therefore useful to contrast farm systems and a lot of confidence can be gained from the use of simulation models.

4.5 Potential as management tool

Some of the challenges in shellfish management concerns finding suitable areas for production with respect to production carrying capacity. In this context this model can provide guidance to questions at the farm scale, such as biomass production potential and geometric dimensions of the farm at potential sites, or simply if a site should be abandoned because of too low background productivity. These questions are of interest for governmental agencies concerned with coastal zone planning an efficient use of coastal areas. The model is planned implemented as a module in a GIS based decision support tool (AKVAVIS, www.akvavis.no) for interactive assessment of site suitability for mussel aquaculture in coastal areas.

Secondly, the model provides information about growth processes at the individual scale, such as size and condition of the mussels, and how these may be influenced by decisions at the farm scale, such as farm geometry, longline spacing and stocking density in the farm (as illustrated in Fig. 7). This is a unique aspect of the present model and this type of information is highly relevant for the farmer who is interested in optimising farm configuration to achieve the best compromise between total mussel biomass production and quality of individual mussels. However, as discussed above the model ignores other important aspects of aquaculture management like *e.g.* economy of farming and interactions between farms and environments. It is tempting to think along the lines of integrated and comprehensive models that enable dynamic linkages of processes at different scales, but complex models are also more demanding to operate and their predictions are usually associated with large uncertainties. Thus, future research should explore the paths of more complex model systems in parallel with simpler narrowly focused models for easy application for non-expert users.

5. Acknowledgements

This work was supported by the Research Council of Norway within the Research Institution-based Strategic Project "Carrying Capacity in Norwegian Aquaculture (CANO)" (grant no 173537) and the Aurora mobility project "Modelling Mussel for Aquaculture (MOMA)" (grant no 187696).

6. References

Aure, J., Strohmeier, T., Strand, O., 2007. Modelling current speed and carrying capacity in long-line blue mussel (*Mytilus edulis*) farms. Aquac. Res. 38, 304-312.

Bacher, C., Black, E., 2008. Risk assessment of the potential decrease of carrying capacity by shellfish farming, GESAMP Reports and Studies. Food and Agriculture Organization of the United Nations, pp. 94-109.

Bacher, C., Gangnery, A., 2006. Use of dynamic energy budget and individual based models to simulate the dynamics of cultivated oyster populations. J. of Sea Res. 56, 140-155.

Bacher, C., Grant, J., Hawkins, A.J.S., Fang, J.G., Zhu, M.Y., Besnard, M., 2003. Modelling the effect of food depletion on scallop growth in Sungo Bay (China). Aquat. Living Resour. 16, 10-24.

Blanco, J., Zapata, M., Moroño, A., 1996. Some aspects of the water flow through mussel rafts. Sci. Marina 60, 275-282.

Boyd, A.J., Heasman, K.G., 1998. Shellfish mariculture in the Benguela system: Water flow patterns within a mussel farm in Saldanha Bay, South Afr.. J. of Shellfish Res. 17, 25-32.

Brigolin, D., Dal Maschio, G., Rampazzo, F., Giani, M., Pastres, R., 2009. An individual-based population dynamic model for estimating biomass yield and nutrient fluxes through an off-shore mussel (*Mytilus galloprovincialis*) farm. Estuar. Coast. Shelf Sci. 82, 365-376.

Brigolin, D., Davydov, A., Pastres, R., Petrenko, I., 2008. Optimization of shellfish production carrying capacity at a farm scale. Appl. Math. Comput. 204, 532-540.

Callier, M.D., Weise, A.M., McKindsey, C.W., Desrosiers, G., 2006. Sedimentation rates in a suspended mussel farm (Great-Entry Lagoon, Canada): biodeposit production and dispersion. Mar. Ecol.-Prog. Ser. 322, 129-141.

Carlsson, M.S., Holmer, M., Petersen, J.K., 2009. Seasonal and spatial variations of benthic impacts of mussel longline farming in a eutrophic Danish fjord, Limfjorden. J. of Shellfish Res. 28, 791-801.

Cugier, P., Struski, C., Blanchard, M., Mazurie, J., Pouvreau, S., Olivier, F., Trigui, J.R., Thiebaut, E., 2010. Assessing the role of benthic filter feeders on phytoplankton production in a shellfish farming site: Mont Saint Michel Bay, France. J. of Mar. Syst. 82, 21-34.

Dame, R.F., Prins, T.C., 1998. Bivalve carrying capacity in coastal ecosystems. Aquat. Ecol. 31, 409-421.

Dolmer, P., 2000. Algal concentration profiles above mussel beds. J. of Sea Res. 43, 113-119.

Dowd, M., 2005. A bio-physical coastal ecosystem model for assessing environmental effects of marine bivalve aquaculture. Ecol. Model. 183, 323-346.

Drapeau, A., Comeau, L.A., Landry, T., Stryhn, H., Davidson, J., 2006. Association between longline design and mussel productivity in Prince Edward island, Canada. Aquac. 261, 879-889.

Duarte, P., Labarta, U., Fernandez-Reiriz, M.J., 2008. Modelling local food depletion effects in mussel rafts of Galician Rias. Aquac. 274, 300-312.

Ferreira, J.G., Hawkins, A.J.S., Bricker, S.B., 2007. Management of productivity, environmental effects and profitability of shellfish aquaculture - the Farm Aquaculture Resource Management (FARM) model. Aquac. 264, 160-174.

Ferreira, J.G., Hawkins, A.J.S., Monteiro, P., Moore, H., Service, M., Pascoe, P.L., Ramos, L., Sequeira, A., 2008. Integrated assessment of ecosystem-scale carrying capacity in shellfish growing areas. Aquac. 275, 138-151.

Filgueira, R., Grant, J., 2009. A Box Model for Ecosystem-Level Management of Mussel Culture Carrying Capacity in a Coastal Bay. Ecosyst. 12, 1222-1233.

Fuentes, J., Gregorio, V., Giraldez, R., Molares, J., 2000. Within-raft variability of the growth rate of mussels, *Mytilus galloprovincialis*, cultivated in the Ria de Arousa (NW Spain). Aquac. 189, 39-52.

Giles, H., Pilditch, C.A., Bell, D.G., 2006. Sedimentation from mussel (*Perna canaliculus*) culture in the Firth of Thames, New Zealand: Impacts on sediment oxygen and nutrient fluxes. Aquac. 261, 125-140.

Grant, J., Bugden, G., Horne, E., Archambault, M.C., Carreau, M., 2007. Remote sensing of particle depletion by coastal suspension-feeders. Can. J. of Fish. and Aquat. Sci. 64, 387-390.

Guyondet, T., Koutitonsky, V.G., Roy, S., 2005. Effects of water renewal estimates on the oyster aquaculture potential of an inshore area. J. of Mar. Syst. 58, 35-51.

Guyondet, T., Roy, S., Koutitonsky, V.G., Grant, J., Tita, G., 2010. Integrating multiple spatial scales in the carrying capacity assessment of a coastal ecosystem for bivalve aquaculture. J. of Sea Res. 64, 341-359.

Heasman, K.G., Pitcher, G.C., McQuaid, C.D., Hecht, T., 1998. Shellfish mariculture in the Benguela system: Raft culture of *Mytilus galloprovincialis* and the effect of rope spacing on food extraction, growth rate, production, and condition of mussels. J. of Shellfish Res. 17, 33-39.

Husa, V., Skogen, M., Eknes, M., Aure, J., Ervik, A., Hansen, P.K., 2010. Oppdrett og utslipp av næringssalter, in: Gjøsæter, H., Haug, T., Hauge, M., Karlsen, Ø., Knutsen, J.A., Røttingen, I., Skilbrei, O., Sunnset, B.H. (Eds.), Fisken og havet, pp. 79-81.

Inglis, G.J., Hayden, B.J., Ross, A.H., 2000. An overview of factors affecting the carrying capacity of coastal embayments for mussel culture. National Institute of Water & Atmospheric Research Ltd PO Box 8602, Riccarton, Christchurch.

Jansen, H.M., Strand, Ø., Strohmeier, T., Krogness, C.I., Verdegem, M., Smaal, A., in press. Seasonal variability in nutrient regeneration by mussel rope culture (*Mytilus edulis*) in oligotrophic systems. Mar. Ecol.-Prog. Ser.

Karayucel, S., Karayucel, I., 2000. Influence of stock and site on growth, mortality and shell morphology in cultivated blue mussels (*Mytilus edulis L.*) in two scottish sea lochs. Isr. J. of Aquac.-Bamidgeh 52, 98-110.

Kooijman, S.A.L.M., 1986. Energy budgets can explain body size relations. J. of Theor. Biol. 121, 269-282.

Kooijman, S.A.L.M., 2000. Dynamic energy and mass budgets in biological systems, Second Edition ed. Cambridge University Press, Cambridge.

Maar, M., Nielsen, T.G., Petersen, J.K., 2008. Depletion of plankton in a raft culture of *Mytilus galloprovincialis* in Ria de Vigo, NW Spain. II. Zooplankton. Aquat. Biol. 4, 127-141.

Mallet, A.L., Carver, C.E., Landry, T., 2006. Impact of suspended and off-bottom Eastern oyster culture on the benthic environment in eastern Canada. Aquac. 255, 362-373.

McKindsey, C.W., Thetmeyer, H., Landry, T., Silvert, W., 2006. Review of recent carrying capacity models for bivalve culture and recommendations for research and management. Aquac. 261, 451-462.

Mitchell, I.M., 2006. In situ biodeposition rates of Pacific oysters (*Crassostrea gigas*) on a marine farm in Southern Tasmania (Australia). Aquac. 257, 194-203.

Petersen, J.K., Nielsen, T.G., van Duren, L., Maar, M., 2008. Depletion of plankton in a raft culture of *Mytilus galloprovincialis* in Ria de Vigo, NW Spain. I. Phytoplankton. Aquat. Biol. 4, 113-125.

Pilditch, C.A., Grant, J., Bryan, K.R., 2001. Seston supply to sea scallops (*Placopecten magellanicus*) in suspended culture. Can. J. of Fish. and Aquat. Sci. 58, 241-253.

Platt, T., Irwin, B., 1973. Caloric Content of Phytoplankton. Limnol. and Oceanogr. 18, 306-310.

Plew, D.R., Enright, M.P., Nokes, R.I., Dumas, J.K., 2009. Effect of mussel bio-pumping on the drag on and flow around a mussel crop rope. Aquac. Eng. 40, 55-61.

Plew, D.R., Spigel, R.H., Stevens, C.L., Nokes, R.I., Davidson, M.J., 2006. Stratified flow interactions with a suspended canopy. Environ. Fluid Mech. 6, 519-539.

Plew, D.R., Stevens, C.L., Spigel, R.H., Hartstein, N.D., 2005. Hydrodynamic implications of large offshore mussel farms. Ieee J. of Ocean. Eng. 30, 95-108.

Pouvreau, S., Bourles, Y., Lefebvre, S., Gangnery, A., Alunno-Bruscia, M., 2006. Application of a dynamic energy budget model to the Pacific oyster, *Crassostrea gigas*, reared under various environmental conditions. J. of Sea Res. 56, 156-167.

Rosland, R., Strand, O., Alunno-Bruscia, M., Bacher, C., Strohmeier, T., 2009. Applying Dynamic Energy Budget (DEB) theory to simulate growth and bio-energetics of blue mussels under low seston conditions. J. of Sea Res. 62, 49-61.

Sara, G., Mazzola, A., 2004. The carrying capacity for Mediterranean bivalve suspension feeders: evidence from analysis of food availability and hydrodynamics and their integration into a local model. Ecol. Model. 179, 281-296.

Simpson, J.H., Berx, B., Gascoigne, J., Saurel, C., 2007. The interaction of tidal advection, diffusion and mussel filtration in a tidal channel. J. of Mar. Syst. 68, 556-568.

Stevens, C., Plew, D., Hartstein, N., Fredriksson, D., 2008. The physics of open-water shellfish aquaculture. Aquac. Eng. 38, 145-160.

Streeter, V., 1961. Handbook of Fluid Dynamics. McGraw Hill Book Company, New York.

Strohmeier, T., Aure, J., Duinker, A., Castberg, T., Svardal, A., Strand, O., 2005. Flow reduction, seston depletion, meat content and distribution of diarrhetic shellfish toxins in a long-line blue mussel (*Mytilus edulis*) farm. J. of Shellfish Res. 24, 15-23.

Strohmeier, T., Duinker, A., Strand, Ø., Aure, J., 2008. Temporal and spatial variation in food availability and meat ratio in a longline mussel farm (*Mytilus edulis*). Aquac. 276, 83-90.

Strohmeier, T., Strand, O., Cranford, P., Krogness, C.I., 2007. Feeding behaviour and bioenergetic balance of *Pecten maximus* and *Mytilus edulis* in a low seston environment. J. of Shellfish Res. 26, 1350-1350.

Tweddle, J.F., Simpson, J.H., Janzen, C.D., 2005. Physical controls of food supply to benthic filter feeders in the Menai Strait, UK. Mar. Ecol.-Prog. Ser. 289, 79-88.

van der Veer, H.W., Cardoso, J., van der Meer, J., 2006. The estimation of DEB parameters for various Northeast Atlantic bivalve species. J. of Sea Res. 56, 107-124.

7. Annex

7.1 The model for flow reduction and seston depletion

The concept of this model is illustrated in Fig. 1. It is assumed that the physical properties are identical along the longline corridors, that water flows parallel to the longlines, and that the friction with farm structures gradually reduces the current speeds downstream of the flow direction. The flow reduction produces a surplus water volume in the farm, which is assumed to be forced out below the farm to maintain the mass balance. Seston filtration by the mussels in combination with reduced water flow is assumed to produce a decreasing seston concentration in the downstream direction at the longlines.

In the following, we consider a volume of water within an elementary box defined by the height of suspended mussel ropes (B_H), its length along the water flow direction (B_L) and its width (B_W). We assume that the current reduction inside a segment is given by the friction force exerted by the mussels on the ropes (Aure et al., 2007). The friction force is a function of the geometric shape of the segment, the friction properties and the current speed, calculated according the Chezy formula (Aure et al., 2007; Streeter, 1961) given by the equation:

$$Fr = -\rho f_K K_c B_L v^2$$

where ρ is the density of seawater, f_K is the frictional constant, K_c the boundary of the channel that faces the water ($K_c = 2B_H$), and v is the current velocity.

We use the classical Navier-Stokes equation for the conservation of momentum:

$$m \cdot \frac{\partial v}{\partial t} + m \cdot v \cdot \frac{\partial v}{\partial x} = Fr$$

where x is the distance along the longline direction, and m the mass of a elementary water element ($\rho\ B_L\ B_H\ B_W$). We assume that the fluid is in steady state (*i.e.* the velocity field does not change over time), which yields:

$$m \cdot v \cdot \frac{\partial v}{\partial x} = Fr$$

which can be rewritten as:

$$\frac{dv}{dx} = -2 \cdot \frac{f_K}{B_W} \cdot v \qquad (i)$$

The solution is therefore:

$$v = v_1 \cdot e^{-\frac{2 \cdot f_K}{B_w} \cdot x}$$

or

$$v = v_1 \cdot e^{-\delta \cdot x} \qquad (ii)$$

with:

$$\delta = \frac{2 \cdot f_K}{B_w}$$

and v_1 is the background velocity.

A similar differential equation can be proposed to describe the seston profile along the longline. Following Bacher et al. (2003) we can write:

$$\frac{\partial S}{\partial t} + v \cdot \frac{\partial S}{\partial x} = -C_t \cdot S$$

where C_t (d^{-1}) is the total clearance rate, equal to the product of individual clearance rate C_r ($m^3\ d^{-1}\ ind^{-1}$) by the density of mussels M (ind m^{-3}). At steady state (v is given by Eq. *ii*), concentration S is equal to:

$$v \cdot \frac{\partial S}{\partial x} = -C_t \cdot S \qquad (iii)$$

The former equation can be solved easily in the case where the biomass of mussels is uniform within the farm. Using Eq. *ii* therefore yields:

$$S = S_1 \cdot e^{\frac{C_t}{v_1 \cdot \delta} \cdot \left(1 - e^{\delta \cdot x}\right)}$$

where S_1 is the background seston concentration. Note that if δ is close to 0 (which would occur if friction is neglected or the distance between parallel longlines is large enough), the previous equation is equivalent to the classical depletion equation:

$$S = S_1 \cdot e^{-\frac{C_t}{v_1} \cdot x}$$

In practice, seston profile will affect mussel growth which, in turn, will make C_t vary within the farm (see the mussel growth model described in the Materials and Methods section for the relation between mussel growth and filtration). The longline is divided in large boxes (e.g. B_L=10 m), and Eqs. *i* and *iii* are solved numerically by considering the sequence of current velocities at the edge of the boxes ($v_1, v_2, ..., v_{N+1}$). For box *n*, we consider the inflow v_n, the outflow v_{n+1} and the average flow within the box $\frac{v_n + v_{n+1}}{2}$. Eq. *i* is rewritten:

$$\frac{v_{n+1} - v_n}{B_L} = -2 \cdot \frac{f_K}{B_W} \cdot \frac{v_n + v_{n+1}}{2}$$

which yields:

$$v_{n+1} = v_n \cdot \frac{1 - \frac{f_K \cdot B_L}{B_W}}{1 + \frac{f_K \cdot B_L}{B_W}}$$

and

$$v_{n+1} = v_1 \cdot \left(\frac{1 - \frac{f_K \cdot B_L}{B_W}}{1 + \frac{f_K \cdot B_L}{B_W}} \right)^n$$

We obtain the seston concentration from Eq. *iii* in a similar way:

$$S_{n+1} = S_n \left(B_A \cdot (v_n + v_{n+1}) - F_n \right) / \left(B_A (v_n + v_{n+1}) + F_n \right) \qquad (iv)$$

Here F_n (m^3 d^{-1}) is the product of the individual clearance rate Cr (m^3 d^{-1} ind^{-1}) by the volume of the box (B_L B_H B_W) and the density M (ind m^{-3}) of mussels in the box, and B_A is the area delimited by the distance between the longlines (box width) and the depth or the vertical ropes (box height). C_r depends on mussel weight and is derived from the food ingestion rate $\dot{p}_X$ (J d^{-1}) which is detailed in the Materials and Methods section.

7.2 Calculation of food depletion

Using the former equations for flow reduction and seston depletion we calculated concentration profiles for two cases: 1) with and 2) without flow reduction and we used the parameters given in the following table:

Parameter name	Parameter value
v_1 (m s^{-1})	0.05
B_W (m)	5
C_t (s^{-1})	2.33 10^{-4}
f_K	0.02

The comparison presented in the following figure clearly shows that depletion is enhanced by flow reduction.

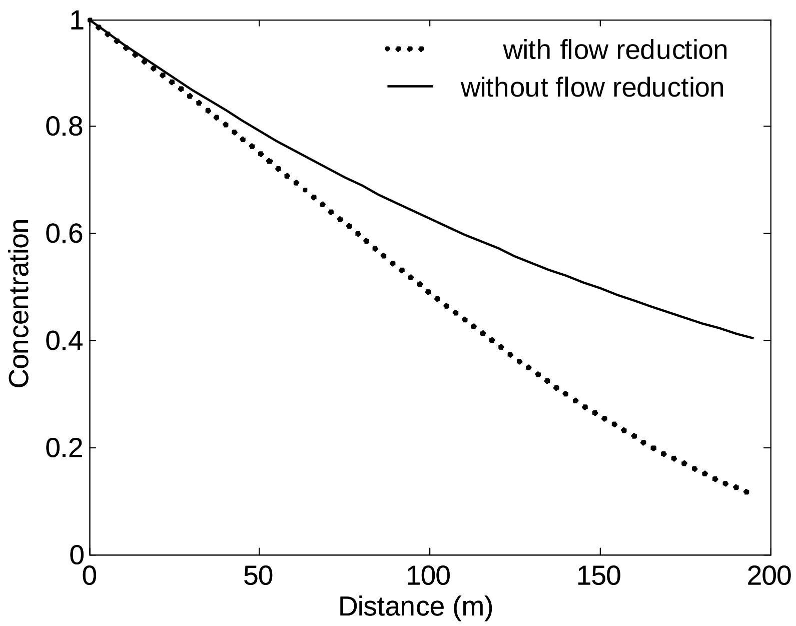

7.3 Calculation of depletion index

By defining the depletion index as the ratio between the renewal time *RT* and the clearance time *CT* we can write:

$$DI = \frac{RT}{CT}$$

$$CT = \frac{V}{CR}$$

$$RT = \frac{V}{FR}$$

where *V* is the volume of water in the farm and *CR* ($m^3\ d^{-1}$) is the total clearance rate by all the mussels in the farm, *FR* ($m^3\ d^{-1}$) is the flow of water through the farm. Now we have

$$FR = v \cdot A$$

$$CR = C_r \cdot M \cdot V = C_t \cdot V$$

with $V = A \cdot L$, where *A* is the cross section and *L* the farm length

We finally get:

$$DI = \frac{RT}{CT} = \frac{CR}{FR} = \frac{C_t \cdot L}{v}$$

In the simple case where there is no current reduction the depletion index is equal to:

$$DI = \log\left(\frac{S_1}{S_L}\right)$$

where S_l is the food concentration at the entrance and S_L the food concentration at the exit of the farm (Petersen et al., 2008).

Figure legends

Figure 1: A longline farm as conceptualised in the model with water and seston flowing along the channel delimited by the longlines and the mussel ropes. The boxes illustrate how the longlines are divided into discrete boxes (n=1 to N) with fixed volumes with: v = currents speed (m d^{-1}), S = seston concentration (mg m^{-3}), F = filtration rate (m^{3} d^{-1}), B_H = box height, B_W = box width, B_L = box length, x = distance in the longline direction.

Figure 2: Environmental data from the Hardangerfjord. The background current (top panel) and chl *a* concentration (middle panel) represent the upper (Hardanger HIGH) and lower (Hardanger LOW) part of the observed ranges at each month. Water temperature (bottom panel) represents the average of the observed ranges at each month.

Figure 3. Simulated water flow (upper row), chl *a* concentrations (mid row) and final mussel flesh mass (bottom row) for a setup with one-way current directions (left column), two-way symmetrical (1:1) current directions (mid column) and two-way skewed (3:1) current directions (right columns) . The lines and markers represent simulations with 1, 2, 3, 5, 7, and 10 m spacing between longlines. Error bars represent variability at different longline positions during the simulation (only displayed for the 3 m spacing).

Figure 4. Upper panel: Simulated shell lengths at the end of the simulation *versus* mean chl *a* concentration over the simulation period; Lower panel: Mean *versus* standard deviation of chl *a* concentration over the simulation period. Only data for the centre and edge positions of the longlines are presented.

Figure 5. Simulated individual dry flesh mass (upper row) and farm biomass (lower row) in response to reduced farm length (150 m) and stocking density (500 ind m^{-2}) (left column) and increased background currents and chl *a* concentrations (right columns). The standard refers to standard farm configuration (Tab. 1) and environmental data from the Lysefjord. Results are displayed for different spacing of the longlines (x-axis). Lines represent mean values; bars represent deviation between longline positions.

Figure 6. Simulated effects of background currents and chl *a* concentration on mussel flesh weight (upper row) and biomass concentration (lower row) for different long-line spacing (x-axis). The flow and chl *a* regime represent the upper (HIGH) and lower (LOW) parts of the environmental ranges in Hardangerfjord.

Figure 7. The isoclines show farm biomass (kg m^{-3}) at different farm lengths (x-axis) and spacing between long lines (y-axis). The left and right panels display biomass at high and low background levels of chl *a*, respectively, while upper and lower panels display high and low stocking density, respectively. The grey area marks combinations of line spacing and farm length which are not in compliance with the criteria for mussel lengths (>28 mm), flesh weight (>0.45 g WW) and normalized spatial size variation (<10%).

TABLES

Table 1. The standard parameter settings of the farm model and half saturation and maximum ingestion rate of the DEB mussel growth model.

Name	Value	Unit	Description
Farm model parameters			
nbox	10	-	Number of modelled sections along farm length
B_H	5.5	m	Vertical extension of stocking lines (hanging from longlines)
B_L	30	m	Length of box
B_W	[1-10]	m	Width of box
F_K	0.02	kg m^{-2}	Friction coefficient between water and farm structures
nmussel	1000	ind m^{-2}	Mussel density at the longline
winit	0.05	g	Initial mussel flesh dry weight
linit	23	mm	Initial shell length
Mussel model parameters			
S_K	1.29	mg chl *a* m^{-3}	Half saturation coefficient
$\{\dot{p}_{Xm}\}$	273	J cm^{-2} d^{-1}	Maximum food ingestion rate by mussels

Table 2. Computation of Depletion Index based on characteristics of shellfish farms documented in several studies. It includes two scenarios from our study corresponding to high current flow, high food concentration and 2 spacings between longlines (1 m, 10 m).

Author	Current velocity (cm s^{-1})	Section (m^2)	Length (m)	Total filtration (m^3 d^{-1})	Flow through the farm (m^3 d^{-1})	Depletion Index	Cultivation system
Bacher et al. (2003)	5.0	1	1000	12960	4320	3.00	Longline
	60.0	1	1000	12960	51840	0.25	Longline
Bacher and Black (2007)	54.0	6000	2500	8352000	279936000	0.03	Longline
Guyondet (2009)	2.0	1	100	80	1728	0.05	Longline
Pilditch et al. (2001)	5.0	1	80	249	4320	0.06	Longline
	5.0	1	500	1555	4320	0.36	Longline
Plew (2005)	5.5	5200	2450	686400	24575616	0.03	Longline
	5.5	5200	2450	4224000	24575616	0.17	Longline
Sara et al. (2004)	3.0	625	9	242611	1620000	0.15	Longline
	3.0	625	23	620006	1620000	0.38	Longline
	15.0	625	32	862618	8100000	0.11	Longline
	15.0	625	70	1886976	8100000	0.23	Longline
Strohmeier et al. (2005)	5.5	165	200	410573	784080	0.52	Longline
Strohmeier et al. (2008)	3.3	165	250	1020730	470448	2.17	Longline
This study	12	5.5	300	112	489	4.30	Longline
	12	55	300	9305	1055	0.20	Longline
Duarte et al. (2008)	3.0	27	20	26244	69984	0.38	Raft
Heasman et al. (1998)	1.3	84	11	423360	90720	4.67	Raft
	3.7	84	11	423360	268531,2	1.58	Raft
	7.6	84	11	423360	551577,6	0.77	Raft
Karayucel and Karayucel	5.2	80	11	34668	359424	0.10	Raft
	5.0	200	27	182347	864000	0.21	Raft
Petersen et al. (2008)	1.5	20	27	19440	25920	0.75	Raft
	4.1	20	27	19440	70848	0.27	Raft

FIGURES

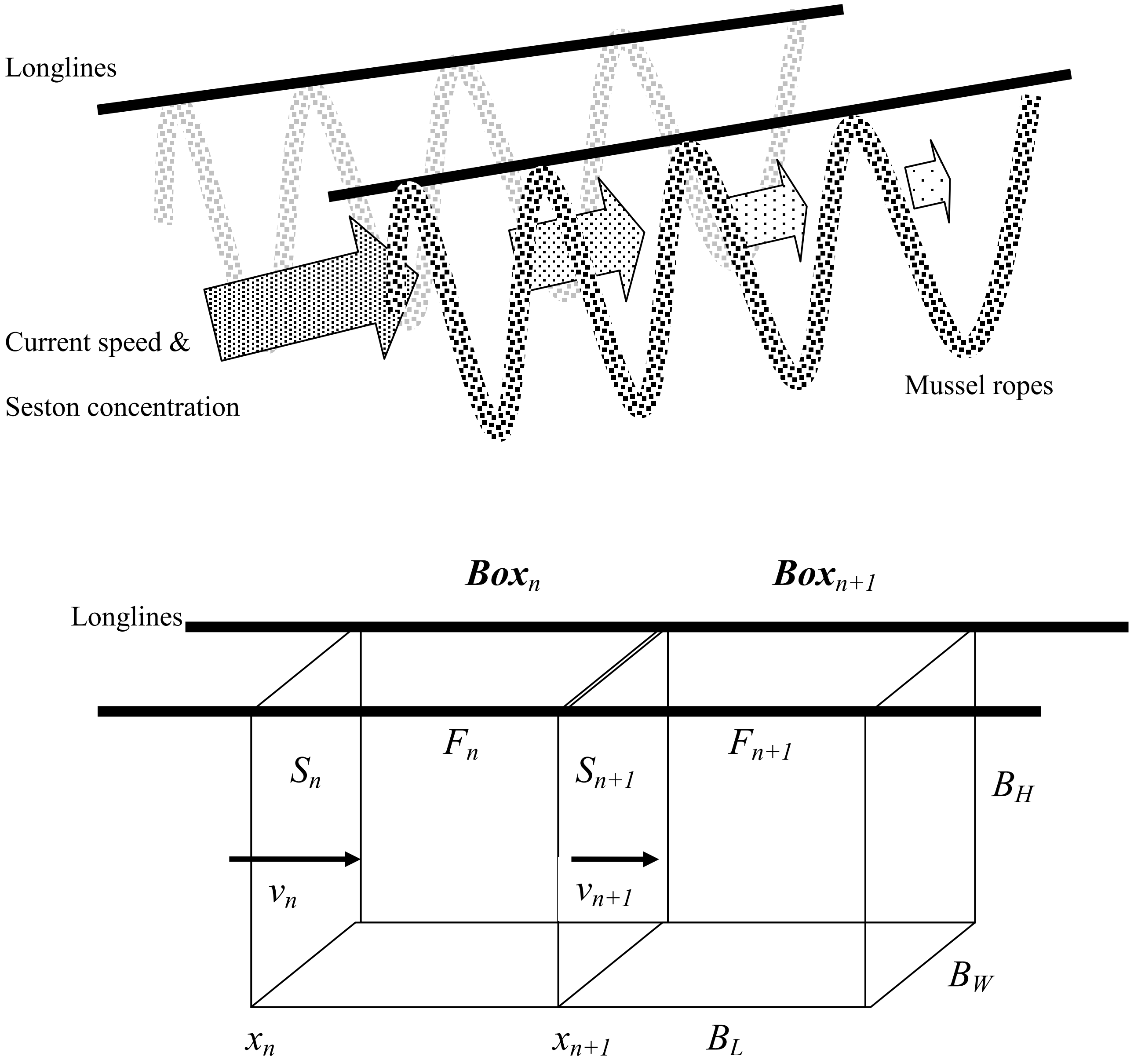

Figure 1

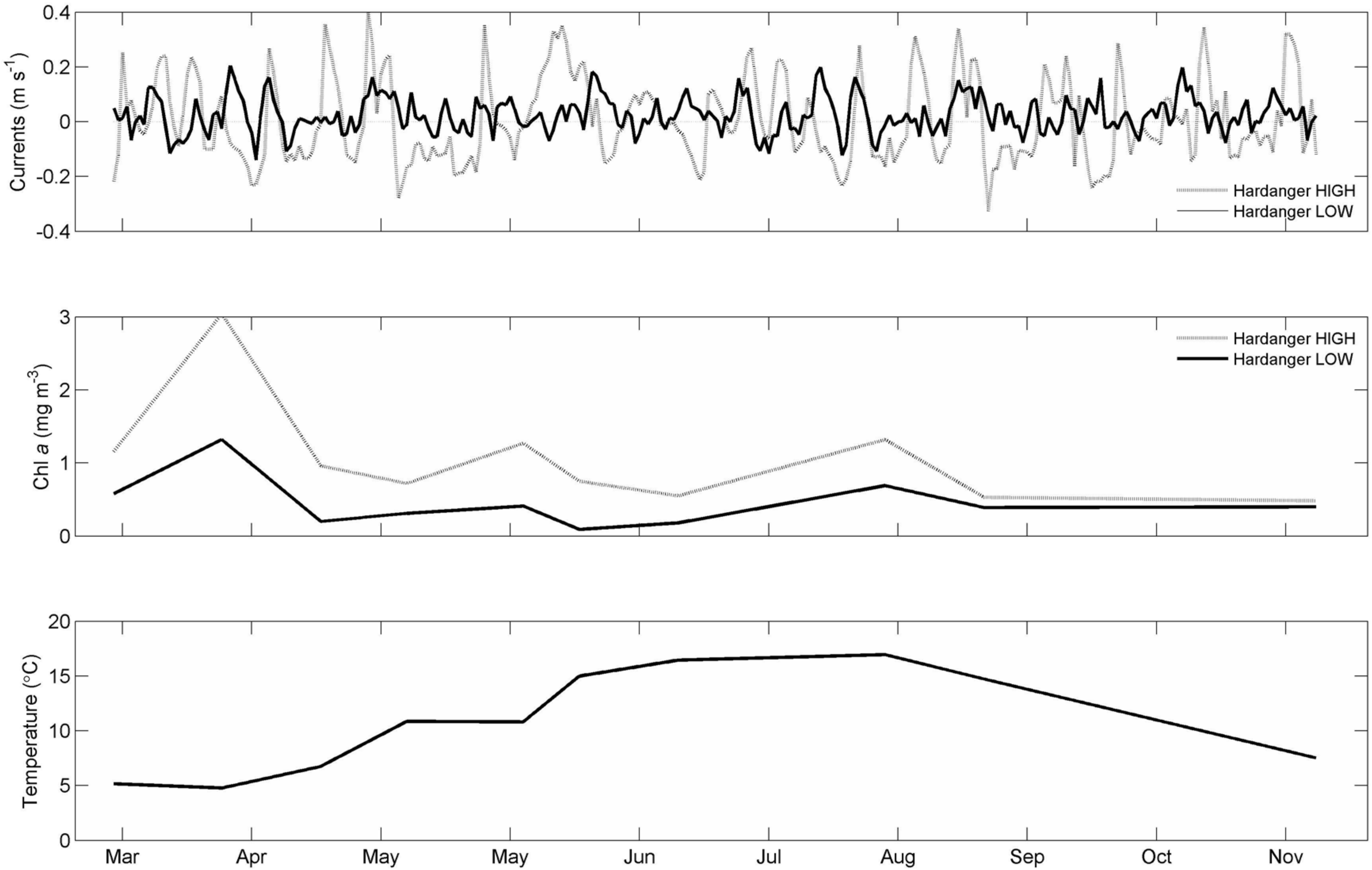

Currents (m s-1)
Hardanger HIGH
Hardanger LOW
Chl a (mg m-3)
Hardanger HIGH
Hardanger LOW
Temperature (°C)
Mar
Apr
May
May
Jun
Jul
Aug
Sep
Oct
Nov

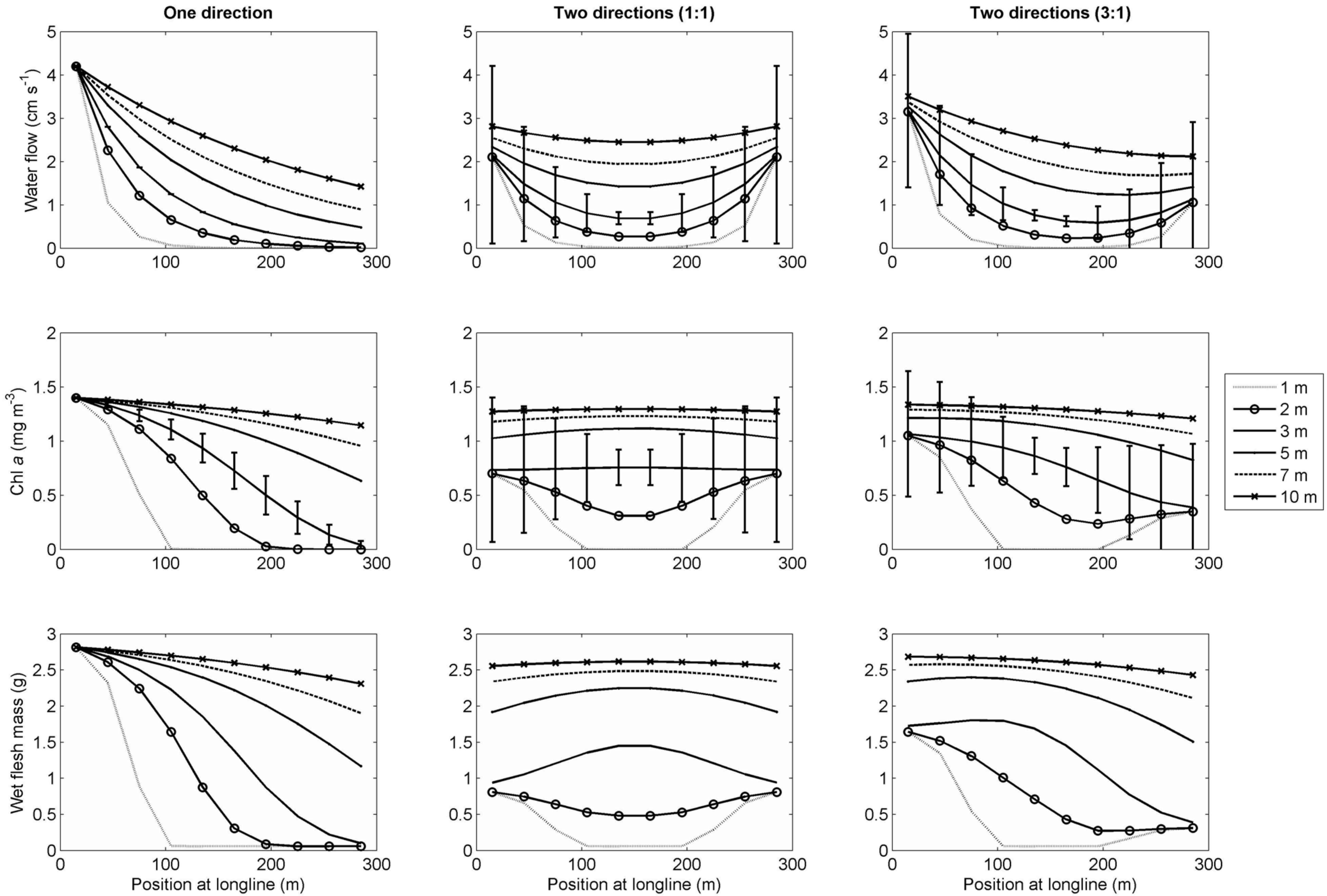

One direction
Two directions (1:1)
Two directions (3:1)
Water flow (cm s-1)
Chl a (mg m-3)
Wet flesh mass (g)
Position at longline (m)
1 m
2 m
3 m
5 m
7 m
10 m

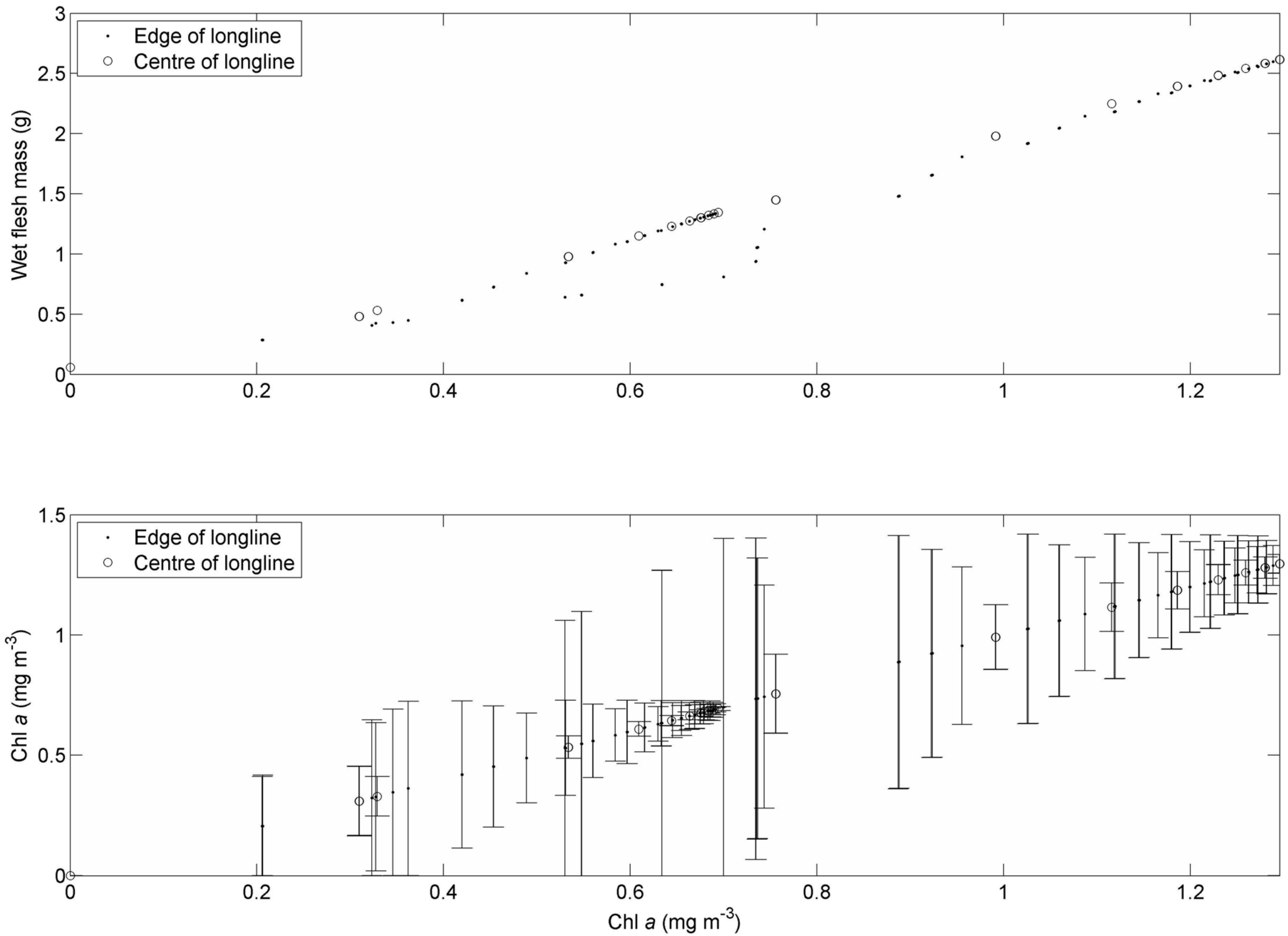

3
2.5
2
1.5
1
0.5
0
Wet flesh mass (g)
Edge of longline
Centre of longline
0
0.2
0.4
0.6
0.8
1
1.2
1.5
1
0.5
0
Chl a (mg m-3)
Edge of longline
Centre of longline
0
0.2
0.4
0.6
0.8
1
1.2
Chl a (mg m-3)

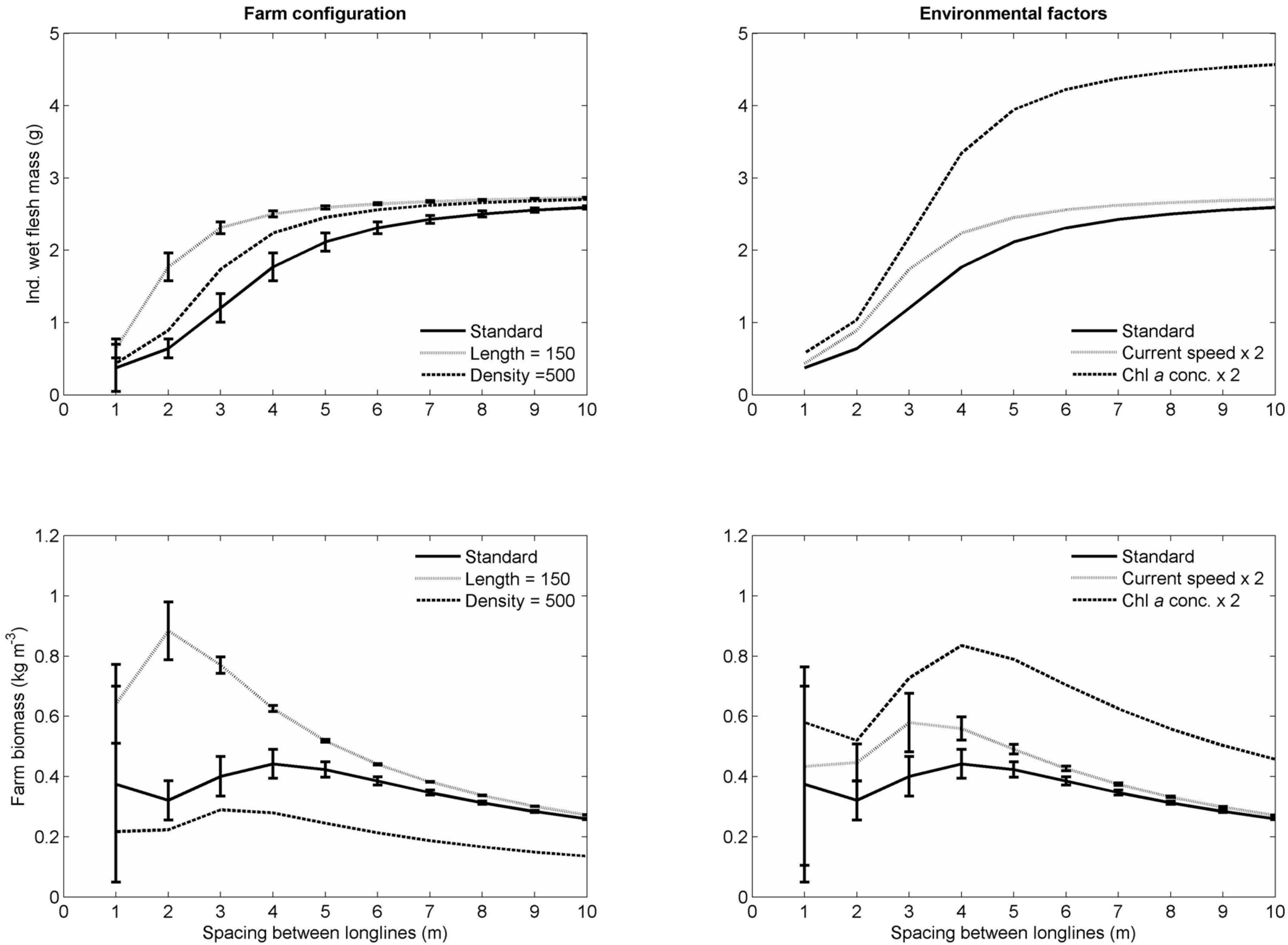

Farm configuration
Environmental factors
Ind. wet flesh mass (g)
Farm biomass (kg m^{-3})
Standard
Length = 150
Density =500
Density = 500
Current speed x 2
Chl *a* conc. x 2
Spacing between longlines (m)

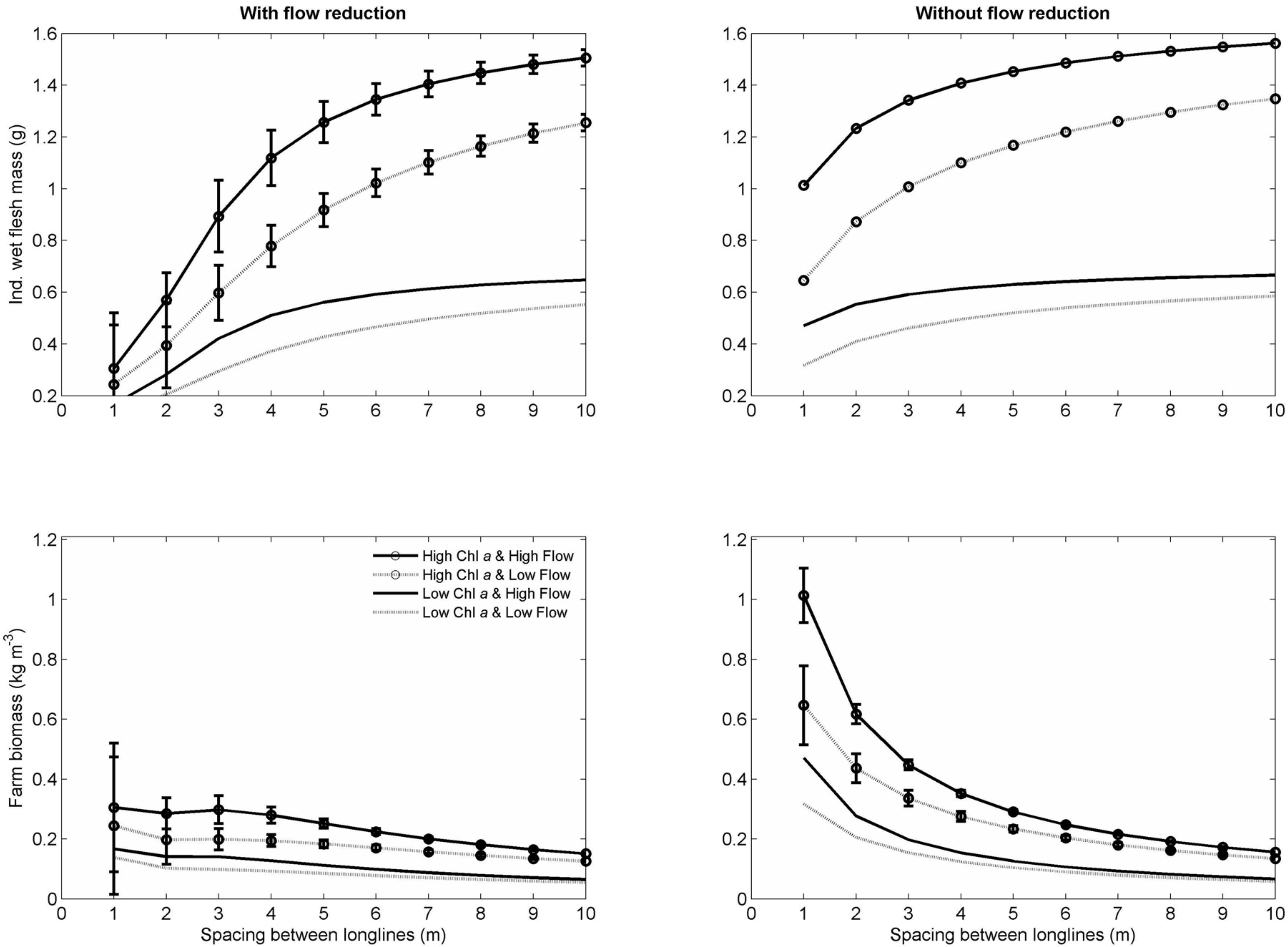

With flow reduction
Without flow reduction
Ind. wet flesh mass (g)
Farm biomass (kg m-3)
High Chl a & High Flow
High Chl a & Low Flow
Low Chl a & High Flow
Low Chl a & Low Flow
Spacing between longlines (m)
Spacing between longlines (m)

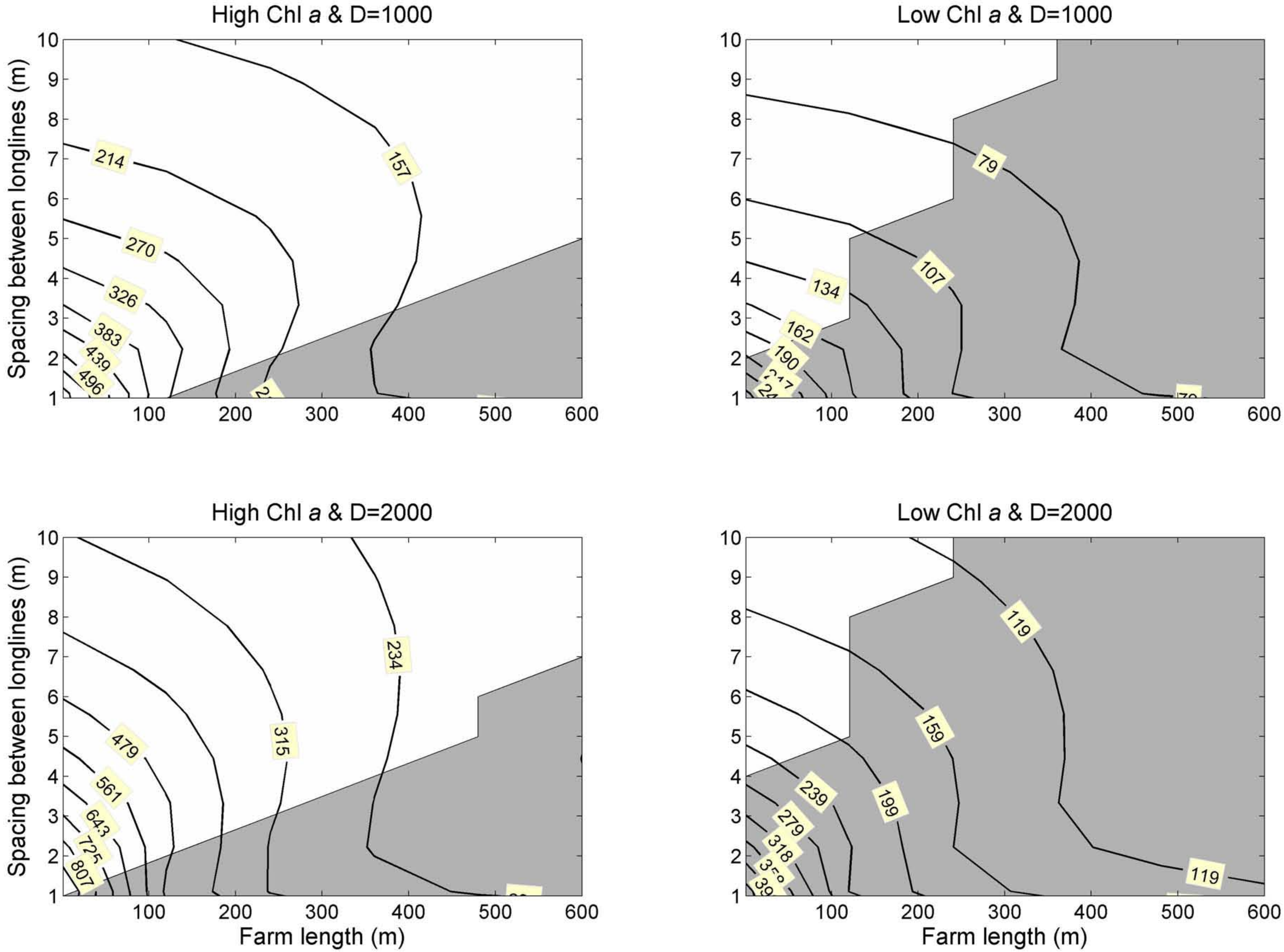
High Chl a & D=1000
Low Chl a & D=1000
High Chl a & D=2000
Low Chl a & D=2000
Spacing between longlines (m)
Farm length (m)
214
270
326
383
439
496
157
79
107
134
162
190
479
561
643
725
807
315
234
119
159
199
239
279
318
119